

## The microstructure effect on the Au/TiO<sub>2</sub> and Ag/TiO<sub>2</sub> nanocomposites photocatalytic activity

D. A. Kozlov<sup>1</sup>, V. A. Lebedev<sup>1,2</sup>, A. Yu. Polyakov<sup>1</sup>, K. M. Khazova<sup>1</sup>, A. V. Garshev<sup>1,2,3</sup>

<sup>1</sup>Faculty of Materials Science, Lomonosov Moscow State University, 1-73 Leninskiye gory, Moscow, 119991, Russia

<sup>2</sup>Faculty of Chemistry, Lomonosov Moscow State University, 1-3 Leninskiye gory, Moscow, 119991, Russia

<sup>3</sup>Baikov Institute of Metallurgy and Material Science RAS, 49 Leninskiy prospekt, Moscow, 119334, Russia

kozlov@inorg.chem.msu.ru, vasya.lebedev@mail.ru, a.yu.polyakov@gmail.com, khazovakm@gmail.com, garshev@inorg.chem.msu.ru

PACS 61.46.+w,68.37.Lp

DOI 10.17586/2220-8054-2018-9-2-266-278

In this work the systematic study of the Au/TiO<sub>2</sub> and Ag/TiO<sub>2</sub> nanocomposites was evaluated. Aeroxide P25 preparation was taken as a titania precursor. Composites were obtained using different wet chemistry techniques: impregnation by previously prepared nanoparticles (NPs) sols, *in-situ* reduction by sodium borohydride, sodium citrate and UV irradiation. The varying of the synthesis method due to the reduction rate differences results in the different interaction between metal NPs and titanium dioxide, and hence different metal/TiO<sub>2</sub> contacts were observed. All the obtained samples were analyzed by XRD, TRS, SEM with EDX and TEM with EDX. According to the statistical analysis of the TEM images the correlation between the metal NPs rate formation and their anisotropy was shown, which may allow us to consider the anisotropy as a descriptor of the contact quality. Combining the results of the optical spectroscopy with the NPs TEM statistical analysis, we confirmed the correlation between observable anisotropy and the contact quality. Finally, the effect of the synthesis method on the photocatalytic activity (PCA) of nanocomposites was shown. Since the work functions of Au and Ag differ, the opposite effects on PCA are expected. Thus, in the case of the Au/TiO<sub>2</sub> nanocomposites, the positive effect associated with NPs anisotropy on the PCA was demonstrated. Alternatively, in the case of the Ag/TiO<sub>2</sub> nanocomposites the PCA evolution was detected only in the case of small NPs formation.

**Keywords:** photocatalysis, titania, nanocomposites, TiO<sub>2</sub>, gold nanoparticles, silver nanoparticles, anisotropy.

Received: 24 January 2018

Revised: 5 February 2018

### 1. Introduction

Currently, photocatalysis is widely used in numerous light-driven technologies, *e.g.* for water purification [1], waste degradation [2–4], water splitting [5] and CO<sub>2</sub> reduction [6]. TiO<sub>2</sub>-based materials are one of the most popular photocatalysts, demonstrating high PCA due to required energy bands positions and an acceptable band gap of 3.2 eV, which corresponds to the near UV range [7]. However, the effective wavelength range for the photocatalysis mediated by pure TiO<sub>2</sub> is limited by UV. PCA of titania-based materials in the visible range can be improved by increasing their absorbance at 400–700 nm wavelengths [8]. For this, the morphology and structure of photocatalyst can be modified by the introduction of dopant additives [9] or accurate (and rather complicated) tuning of the shape of titania NPs [10, 11]. At the same time, large-tonnage production of commercial TiO<sub>2</sub> catalysts, such as Aeroxide P25, is based on the pyrolysis of titanium compounds [12, 13]. Therefore, post-processing modification of TiO<sub>2</sub> NPs is more economically feasible for production of visible-range photocatalysts. Such methods include design of the contact titania with other materials, *e.g.* metal and semiconductor NPs, carbon-based materials, dye molecules. The main disadvantage of the carbon-modified titania is a significant shading and loading of the photocatalyst surface, since optimal carbon materials addition is usually 20–30% that can affect on the absorption ability [8]. Dye-sensitized titania is widely applied for the solar cells [14], but suffers significantly from the photocatalytic dye degradation.

Loading of the titania surface with semiconductor NPs results in a visible-light induced PCA and increases the total (UV and visible) PCA in the case of II-type heterojunction formation. As demonstrated in our earlier article [15], the PCA of nanocomposite based on Aeroxide P25 and WO<sub>3</sub>·H<sub>2</sub>O was increased by *ca.* 30% higher in comparison with the pristine Aeroxide P25. Similarly, Han et al. [16] reported PCA increasing upon loading TiO<sub>2</sub> with semiconductor Cu<sub>2</sub>O NPs. However, modification of titania with metal NPs (such as Ag, Au, Pd, Pt, Cu) is known to be much more effective for achievement of PCA in visible range [17–19].

The formation of the Schottky contact between the metal and semiconductor components of the nanocomposite may increase PCA due to an interparticle charge carriers transfer [20] leading to the spatial separation and, hence, longer lifetimes of photogenerated nonequilibrium electrons and holes. The ohmic contact formation does not result in the charge carriers separation, and hence increase of the PCA is not expected. Moreover, there are few possible mechanisms [21] of energy transfer from plasmonic NPs to the semiconductor, which beneficially effects PCA. According to the work functions of bulk gold and anatase, which are 5.23 eV [22] and 5.10 eV [23] respectively, we can expect Schottky contact formation in this case, whereas Ag/TiO<sub>2</sub> contact should be ohmic due to work function of silver, which is 4.25–4.37 eV [24]. Based on the bulk materials band structure, the principal scheme of the Au/TiO<sub>2</sub> and Ag/TiO<sub>2</sub> contacts are presented on the Fig. 1.

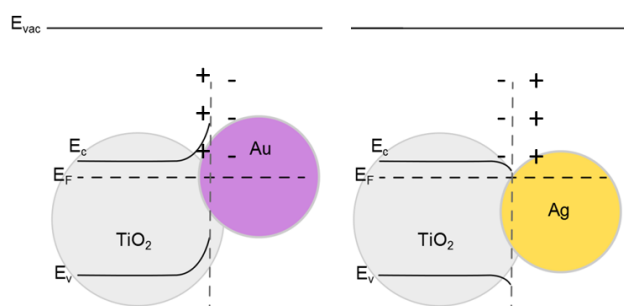


FIG. 1. Principal scheme Au/TiO<sub>2</sub> and Ag/TiO<sub>2</sub> contacts structures based on the bulk materials work functions

At the same time, many authors declared the positive effect of silver NPs on the PCA of titanium dioxide. Some recent reports addressing the Ag NPs effect on the PCA of TiO<sub>2</sub> are summarized in the Table 1. It should be noted that a significant increase (1.5–2 times) is observed mainly for the <10 nm NPs. Alternatively, in the case of larger NPs, the nanocomposites demonstrated decreased PCA. This observation can be explained by a significant increase of Fermi level in silver NPs, which was confirmed elsewhere [25] by Kelvin probe microscopy of gold and silver NPs. Similar size effect was observed by Cozzoli et al. [26], namely the PCA increase was associated with the charge carriers separation observed only in the case of 8–10 nm silver NPs. The measurements of the equilibrium potential of irradiated Au/TiO<sub>2</sub> nanocomposites reported by Subramanian et al. [27] revealed a size-related shift of Fermi level in Au NPs. The greater shift of the Fermi level was observed in smaller Au NPs (20 mV for 8 nm diameter, 40 mV for 5 nm and 60 mV for 3 nm Au NPs) and caused the increase of PCA.

The shape and size variations primarily effect on the optical properties of plasmonic NPs due to the changes of the surface plasmon resonance (SPR) parameters. Particullary, red shift of the SPR wavelength was observed upon increasing the diameter of gold nanospheres [42]. Eustis et al. [43] showed that the increase of the aspect ratio of anisotropic elliptical gold particles also leads to an increased SPR wavelength. A number of methods were developed for mathematical simulation of light scattering and absorption by plasmonic NPs, *e.g.* Discrete Dipole Approximation (DDA), Finite Element Methods (FEM). Several analytical methods (Mie theory, quasistatic theory) [44] were also reported. Kelly et al. [45] used DDA and analytical methods to calculate theoretically the effect of different factors (size, medium permittivity, aspect ratio) affecting the SPR peak position. Therefore, the red shift of the SPR peak position can be caused by increasing of the NPs diameter, aspect ratio, refractive index of the medium, whereas blue shift may be caused by snipping of the non-spherical particles.

As shown above, the effect of plasmonic NPs size on PCA of TiO<sub>2</sub> is studied rather well. At the same time, the impact of the contact between Au or Ag and TiO<sub>2</sub> counterparts has insufficient experimental confirmation. Here we employed different synthesis techniques, namely impregnation with pre-synthesized NPs, reduction of Ag<sup>+</sup> and AuCl<sub>4</sub><sup>-</sup> ions with sodium borohydride (rapid reaction), as well as sodium citrate and UV irradiation (slower reactions) to produce the series of Au/TiO<sub>2</sub> and Ag/TiO<sub>2</sub> nanocomposites. We used TEM to characterize the NPs morphology and to estimate the shape anisotropy which was chosen as a simplified descriptor of the contact quality. These data were compared with the measured and simulated UV-visible-NIR absorption spectra of the nanocomposites. The composition and structure of the nanocomposites was also studied by XRD, SEM-EDX and STEM-EDX. Finally, we discussed the impact of plasmonic NPs morphology (effective size, shape anisotropy) and their contact with TiO<sub>2</sub> on the PCA of the designed nanocomposites.

TABLE 1. The articles review data of the metal nanoparticles size effect on the PCA of Ag/TiO<sub>2</sub> nanocomposite

Ag NPs size	Method of PCA measurement*	Relative increase of PCA	Ref
1–2 nm	MO Photodegradation	1.15	[28]
1.5–2 nm	Phenol photodegradation	1.5	[29]
2 nm	Photodegradation of acetone	1–1.2	[30]
2–4 nm	RhB Photodegradation	1.5	[31]
3 nm	MB Photodegradation	3.7	[19]
3 nm	Photodegradation of Safranin-O	1.6	[32]
3–5 nm	Photodegradation pentachlorophenol	2	[33]
5 nm	MB Photodegradation	2.8	[19]
5 nm	MB Photodegradation	Visible light irradiation	[34]
7 nm	Selective oxidation of benzyl alcohol	2	[35]
7 nm	RhB Photodegradation	2	[36]
8 nm	MB Photodegradation	2	[19]
9 nm	MO Photodegradation	1.2	[37]
7–10 nm	MB Photodegradation	1.1	[38]
10 nm	Catalytic oxidation of benzene	None	[39]
20 nm	MO Photodegradation	1.5	[40]
24 nm	RhB Photodegradation	Visible light irradiation	[41]

\*MB – Methylene Blue, MO – Methyl Orange, RhB – Rhodamine B

## 2. Simulation

To determine the SPR peak position position in the media with different permittivity, we calculated the dependence of the extinction cross sections on the wavelength for gold and silver NPs with a diameter of 20 nm. The calculation was provided by the Mie theory:

$$\sigma(\lambda) = \frac{24\pi^2 a^3 \sqrt{\varepsilon_m^3(\lambda)}}{\lambda \ln 10} \cdot \left[ \frac{\varepsilon_i(\lambda)}{(\varepsilon_r(\lambda) + 2\varepsilon_m(\lambda))^2 + \varepsilon_i(\lambda)^2} \right], \quad (1)$$

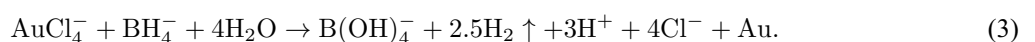
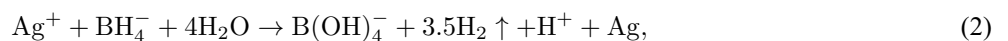
where  $a$  – a particle size,  $\varepsilon_i(\lambda)$  and  $\varepsilon_r(\lambda)$  – imaginary and real parts of the NPs material permittivity as a function of a wavelength, and  $\varepsilon_m(\lambda)$  – a permittivity of the medium.

The DDA modelling were performed using the DDSCAT software [46]. Values of the real and imaginary parts of the complex dielectric permittivity of gold and silver were taken from the article [47] in the both cases. Size of model particle was chosen at least of 30000 dipoles. Effective size was recalculated as  $a_{eff} = \frac{1}{2} \cdot d_{eff}$ . To reduce the angular dependency, for each  $\lambda$ ,  $d_{eff}$  nine target orientations were averaged for two incident polarizations.

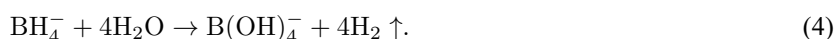
## 3. Experimental

### 3.1. Synthesis

*3.1.1. Reduction with sodium borohydride.* Aqueous solutions of gold or silver precursors (HAuCl<sub>4</sub> or AgNO<sub>3</sub>, respectively) were added to reach the metal amount of 5% w.p. in the final nanocomposite. The pH value was adjusted by drop-wise addition of 2M NaOH or HNO<sub>3</sub> solutions and was measured by ESK 10601/7 electrode, filled with NH<sub>4</sub>NO<sub>3</sub> solution to prevent the seepage of chlorine ions to the mixture. Samples were obtained only in the acidic media (pH 2–6) due to oxide and hydroxide precipitation possibility in the case of silver and basic reduction in the case of gold [48]. After the pH adjustment, suspension was stirred for the 30 min, and then a fresh ice-cold NaBH<sub>4</sub> solution was added with 30% molar excess relative to the metal ions concentration. The principal reactions may be written as follows:

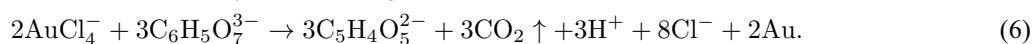
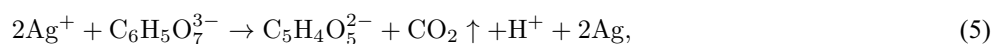


The side process of sodium borohydride hydrolysis may be described as follows [49]:



In the case of AuCl<sub>4</sub><sup>-</sup> reduction, the solution color was changed from light-yellow to dark red-wine over 3–5 min. This corresponds to the relatively rapid formation of gold NPs. In the case of Ag<sup>+</sup> reduction, the colorless solution becomes yellowish brown in a similar timeframe as in the case of gold. The obtained products were separated by centrifugation (8000 rpm, 15 min), and triple rinsed with the DW (160 ml each time). The final precipitate was dried at 80°C during 12 h. It should be noted, that rinse water was colorless, and the absence of observable concentration of metal NPs in the rinse water is the evidence of the nanocomposite formation. Samples obtained using this method were labelled as Au/TiO<sub>2</sub> (b) and Ag/TiO<sub>2</sub> (b).

**3.1.2. Reduction with sodium citrate.** Syntheses utilizing sodium citrate as a reducing agent were evaluated by the similar method: DW solution of sodium citrate was added to the titania aqueous suspension with the metal precursor. During the reduction process temperature was maintained at 90°C to increase the reaction rate. The ratio of metal ions and sodium citrate was about 1:9. In the case of gold NPs formation, it took about 20 min to change color of the reaction solution from yellow to light violet. In the case of silver NPs formation the reaction was carried out for 6 h and the color of reaction mixture was changed from colorless to dark brown. The principal reactions of the metal ions reduction by the citrate anions may be written as follows [50–52]:



The obtained products were separated, washed and dried under same conditions. The rinse water was colorless as well as in the case of reduction by borohydride. Samples obtained using this method were labelled as Au/TiO<sub>2</sub> (cit) and Ag/TiO<sub>2</sub> (cit).

**3.1.3. Reduction with UV light.** To functionalize titania with metal NPs under UV light, an aqueous suspension of titania, included 20 mg titania powder with 100 ml of metal precursor solution (concentration corresponded to 5% w.p. of metal in the final product), was irradiated by the UV lamp MADIX Y1207 (electric power 20 W) under a vigorous stirring. In the case of Ag/TiO<sub>2</sub> nanocomposites, the suspension was irradiated for 20 min, whereas in the case of Au/TiO<sub>2</sub>, the reaction could be as long as 3 h. The completion of reaction was indicated by the finishing of the color changing. Then, samples were separated by the centrifugation, washed and dried under same conditions. Samples obtained using this method were labelled as Au/TiO<sub>2</sub> (UV) and Ag/TiO<sub>2</sub> (UV).

**3.1.4. Reference samples.** Au/TiO<sub>2</sub> and Ag/TiO<sub>2</sub> nanocomposites were also prepared by mixing of the titania suspension with previously prepared gold or silver NPs sols. Metals NPs sols syntheses were carried out at same condition as in the case of citrate reduction, but without the presence of titania. To obtained mixtures containing metal and semiconductor NPs were freeze-dried using a liquid nitrogen and then freeze-dried by Labconco Freezone lyophilizer. Dried samples were washed with the centrifugation in DW water. Since rinse water after the sample precipitation was also colorless, we assume that non-redispersibility of NPs was caused by the formation of nanocomposite of metal NPs with titania. Samples obtained using this method were labelled as Au/TiO<sub>2</sub> (imp) and Ag/TiO<sub>2</sub> (imp).

## 3.2. Analysis

**3.2.1. X-Ray Diffraction.** Phase composition of the nanocomposites was investigated by the X-ray Diffraction (XRD) at CuK<sub>α</sub> radiation on the Rigaku D/MAX 2500 diffractometer with the rotating anode. X-Ray patterns were collected at the 10–90°2θ range, 0.02°2θ step, with 1 s acquisition in each point. To deconvolute titania, gold and silver peaks 30–50°2θ range was investigated with the 10 s acquisition at each point. XRD profile analysis were performed using Jana2006 [53] software. The coherent scattering region (CSR) sizes  $d_{CSR}$  were calculated by the Sherrer equation.

**3.2.2. ζ-potential measurement.** ζ-potentials of the aqueous nanocomposite suspensions were measured using Zetasizer Nano ZS. Titania P25 suspension was adjusted to the required pH value (pH of 3–9 range) by the drop-wise addition of 2M HCl and NaOH solutions and then 1 ml of obtained suspension was transferred into the Malvern Instruments DTS1070 cell. Measurement was performed in the transmission geometry using standard 633 nm laser and 17° scattering measurement angle.

**3.2.3. Total reflectance spectroscopy.** The total reflectance spectra (TRS; both diffuse and specular reflectance) of synthesized nanocomposites were registered in UV-visible-NIR range using Lambda 950 (Perkin Elmer) spectrophotometer (wavelength range of 300–1000 nm, with 1 nm step). The spectra were collected using Spectralon-coated integrating sphere (150 mm diameter). The samples were placed to the reflectance port of the sphere. White Spectralon standard was used to collect 100% total reflectance reference. The registered TRS were recalculated to the absorbance using the standard software of the spectrophotometer.

**3.2.4. Electron Microscopy.** The Scanning Electron Microscopy (SEM) images and energy-dispersive X-ray spectra (EDX) were recorded on a Supra 50VP (Leo), equipped with EDX X-MAX 80 detector and INCA software (Oxford Instruments Inc.). Transmission Electron Microscopy (TEM) Bright Field (BF) images and the corresponding EDX maps were obtained on the Libra 200MC (Zeiss) microscope operating at 200 kV and equipped with EDX X-MAX 80T detector and the AZtec software (Oxford Instruments Inc.). The TEM images were analyzed with the Gwyddion software [54] to calculate the size and shape distributions of NPs. Observed NPs were approximated as elliptical particles, so the lengths of  $a$  and  $b$  pair axes for each ellipse were measured (see the scheme on Fig. 2).

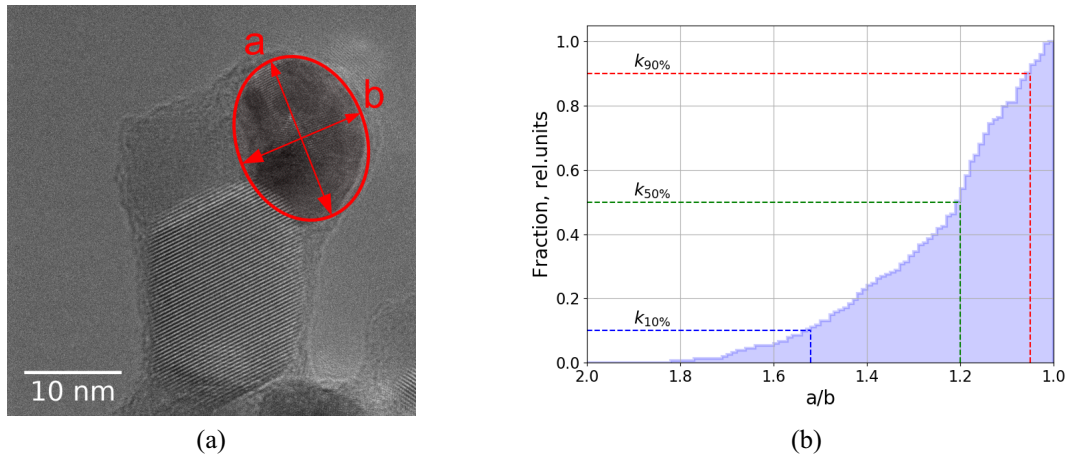


FIG. 2. (a) Au/TiO<sub>2</sub> (cit) TEM BF image with scheme of the particle size measurements,  $a$  and  $b$  – elliptical axes. (b) Normalized negative cumulative distribution

For each particle the effective size  $d_{eff}$  was calculated as a diameter of the sphere with the same volume:

$$d_{eff} = \sqrt[3]{a \cdot b^2}. \quad (7)$$

After that the  $d_{eff}$  distributions were calculated with the step of 1 nm using *scipy* and *Matplotlib* software [55, 56]. The parameters of Gauss fits for the obtained size distributions are presented in Table 2.

TABLE 2. Statistical parameters of the nanocomposites

Sample	CSR, nm	$d_{eff}, \text{nm}$	$\omega_{eff}$	$k_{90\%}$	$k_{50\%}$	$k_{10\%}$	$\lambda_{SPR}$
Au/TiO <sub>2</sub> (imp)	25	30	4	1.02	1.11	1.28	557
Au/TiO <sub>2</sub> (b)	7	11	6	1.01	1.12	1.33	544
Au/TiO <sub>2</sub> (cit)	17	22	7	1.04	1.17	1.37	537
Au/TiO <sub>2</sub> (UV)	15	17	5	1.03	1.16	1.43	550
Ag/TiO <sub>2</sub> (imp)	20	16	6	1.02	1.11	1.30	440
Ag/TiO <sub>2</sub> (b)	7	13	4	1.01	1.10	1.30	438
Ag/TiO <sub>2</sub> (cit)	14	20	11	1.05	1.20	1.52	447
Ag/TiO <sub>2</sub> (UV)	23	21	8	1.05	1.22	1.46	453

To reveals the observable anisotropy of metal NPs, the negative cumulative distribution of  $k = a/b$  value was calculated with the step of 0.01. Based on this distribution, there were calculated the  $k_{10}$ ,  $k_{50}$  and  $k_{90}$  values, which corresponds to the 10%, 50% and 90% amount of NPs with anisotropy higher than  $k$ .

### 3.3. PCA measurements

The photocatalytic activity of the samples was measured by the decolorization of a methyl orange (MO) dye solution. For that, 2–3 mg of the sample were dispersed in 8 ml of DW by the ultrasonic treatment and placed into the thermostated (40°C) AceGlass reactor. Part of measurements were repeated with the use of phosphate buffer (pH 6.9) instead of DW. The 7 ml of 0.3 mM MO solution was added after 10 minutes. The concentrations in the suspension was of 0.14 mM/l of MO and 130–200 mg/l of catalyst. After the next 10 min, the suspension was irradiated by 5W high pressure Hg lamp. The photocatalytic experiments were performed for 3 hours. During the experiment, the reaction mixture was pumped through Malvern Instruments DTS1070 cell, where the absorption spectra was acquired every 3 s using the xenon HRX-2000 lamp and Ocean Optics QE65000 spectrometer. The details of experimental setup and data processing are described in our previous articles [15,57]. In the work [57], we demonstrated, that in the case of this set up the obtained data of the MO decoloration corresponds to the oxidative photodegradation of MO. The initial titania (Aeroxide P25) was used as a reference in all the measurements. The PCA value  $PCA_S$  for the sample  $S$  was calculated from the MO decolorization rate  $r_S$  in the normalization on the sample weight  $m_S$  as follows:

$$PCA_S = \frac{r_S/m_S}{r_{P25}/m_{P25}} \cdot 100\%. \quad (8)$$

The value of  $r_{P25}/m_{P25}$  for the used setup was of 0.09 mg<sup>-1</sup>·h<sup>-1</sup> for the buffer solution and of 0.14 mg<sup>-1</sup>·h<sup>-1</sup> for the DW. The use of inorganic buffer solution for PCA measurements allows one to reach the stability of pH value during the photodegradation process, which is preferable in the case of the decolorization rate measurements for the pH-sensitive dyes. Moreover, for the PCA measurements of titania and titania-based nanocomposites, the phosphate buffer solution significantly improve the suspension stability.

Such effect is not too obvious: it is well-known, that the point of zero charge (PZC) for titania is about of the pH 6–7, and the pH of phosphate buffer solution is pH 6.9. Besides, due to the adsorption of phosphate anions on the titania surface and the following changes in  $\zeta$ -potential, the aggregation ability in the case of DW is more than in the case of buffer solution. Measured values of  $\zeta$ -potential for P25 titania suspension with different pH, compared to the same for phosphate buffer solution are shown in Fig. 3. However, due to the phosphate anions adsorption, measured PCA value significantly decrease and it should be taken into the account during the measurements [58–60].

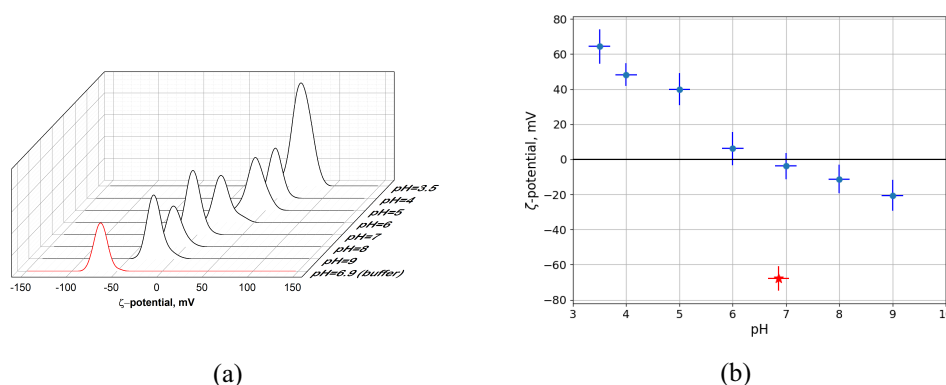


FIG. 3. (a)  $\zeta$ -potential distributions and (b) pH dependency of  $\zeta$ -potential for the titania suspension in DW and phosphate buffer solution (red curve). The red dot corresponds to the  $\zeta$ -potential value in the buffer solution

## 4. Results and discussion

Wet chemistry techniques are widely used for silver and gold NPs decolorization of titania [8, 27, 35, 41] and other semiconductors [61]. Among these techniques, the most popular are impregnation of semiconductor powder by previously synthesized metal NP sols and *in situ* growth of NPs on the semiconductors surface. The latter is usually based on reduction of dissolved Au(III) and Ag(I) compounds. The rate of reduction has a strong impact on the morphology of obtained metal NPs. Additionally, it may determine the type of nucleation (homogeneous or heterogeneous) and, hence, the contact quality between metal and semiconductor counterparts in

final nanocomposites, affecting their properties. Therefore, here, we used different rates of  $\text{HAuCl}_4$  and  $\text{AgNO}_3$  reduction in the presence of titania suspension. For the rapid reduction we employed sodium borohydride, whereas slower reduction was provided by sodium citrate and UV irradiation. Moreover, to tune the reduction rate using citrate anions, the reaction mixture additionally was heated to increase the rate of reduction, whereas in the case of a borohydride anions in this work used an ice-cold solution to slow it down. The reduction by photogenerated charge carriers [62] was used to increase the contact effect on the nanocomposites properties via directly NPs formation on the semiconductor surface. Photoexcited electrons reduce the metal ions adsorbed on the semiconductor surface, and hence this reduction method leads to heterogeneous nucleation. In the case of the rapid reduction, which we can observe using borohydride anions, we can expect a homogeneous nucleation and the formation of a weak metal/semiconductor contact. Therefore, in this case metal NPs have a lower effect on the properties of the obtained nanocomposites. Using citrate anions and UV irradiation the rate of reduction is low, and hence the heterogeneous nucleation and a better contact formation should be expected.  $\text{Au/TiO}_2$  and  $\text{Ag/TiO}_2$  nanocomposites prepared by impregnation technique were used as reference samples.

#### 4.1. Size and morphology

The TEM BF images of the synthesized nanocomposites are shown on Fig. 4 and Fig. 5. All the employed techniques resulted in appearance of gold or silver NPs distributed on the surface of titania NPs (40 nm for both anatase and rutile phases). The results for  $\text{Au/TiO}_2$  and  $\text{Ag/TiO}_2$  nanocomposites obtained by the impregnation of titania powder with previously synthesized NPs demonstrate that this method results in a narrow distribution of NPs sizes, but generally, the nanocomposites include aggregated NPs as at Fig. 4a and Fig. 5a. The presence of suspended titania particles may initiate the aggregation process of the initially stable metal NPs aqueous colloid suspension. Generally, to prevent the NPs aggregation, it may be reasonable to use well-stabilized water redispersible metal NPs, stabilized by humate polyanions [50], but the use of stabilizing agents affects on the metal/semiconductor contact due to the organic interlayer, and hence obtained materials are not applicable in photocatalysis.

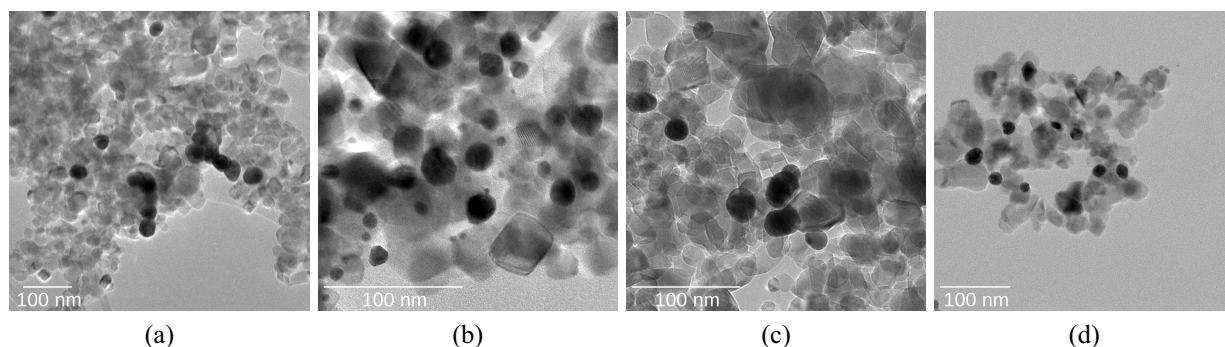


FIG. 4. TEM BF images of the nanocomposites: (a)  $\text{Au/TiO}_2$  (imp), (b)  $\text{Au/TiO}_2$  (b), (c)  $\text{Au/TiO}_2$  (cit), (d)  $\text{Au/TiO}_2$  (UV)

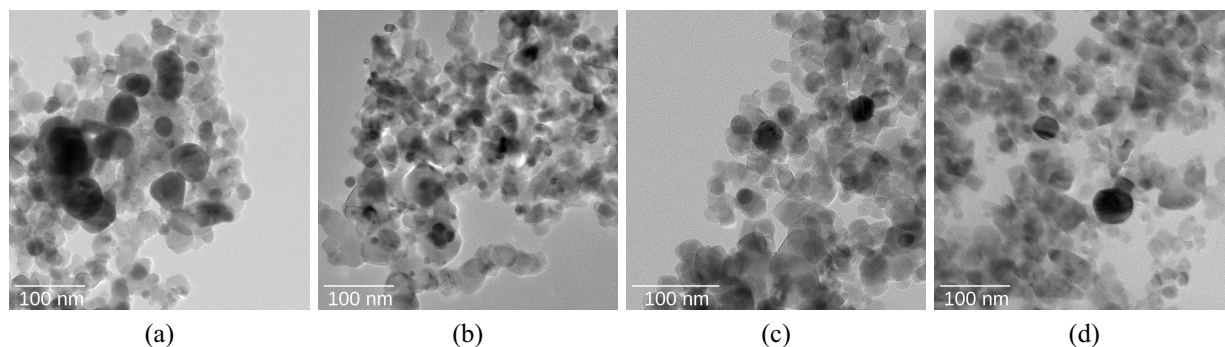


FIG. 5. TEM BF images of the nanocomposites: (a)  $\text{Ag/TiO}_2$  (imp), (b)  $\text{Ag/TiO}_2$  (b), (c)  $\text{Ag/TiO}_2$  (cit), (d)  $\text{Ag/TiO}_2$  (UV)

To quantify the particles size and compare the anisotropy of NPs, a statistical analysis was performed. The average effective diameters of metal NPs were calculated for all samples and are presented in the Table 2. In the case of nanocomposites obtained with the reduction by borohydride the averaged diameter of the metal NPs is significantly smaller both for gold and silver (11–13 nm) that in the case of reduction by citrate and UV (20–22 nm). According to the calculated cumulative anisotropy distributions  $k_{10\%}$ ,  $k_{50\%}$ , and  $k_{90\%}$  values were determined and are presented in the Table 2. In the case of reduction with sodium borohydride and deposited by impregnation metal NPs anisotropies are smaller that in the case of the citrate and UV irradiation syntheses methods. These differences may be caused by the reduction rate differences. Rapid reduction with the borohydride results in the high probability of the homogeneous nucleation, but in the case of slow reduction with the citrate and especially UV irradiation it leads to the heterogeneous nucleation on the surface of titania particles. Therefore, such anisotropy may indicate the contact quality. The differences in the anisotropies of metal NPs, obtained by a citrate reduction with and without titania presence may serve as an additional evidence of the heterogeneous nucleation. In the case of the titania presence, the anisotropy of metal NPs is higher, that in the case of reduction without the titania, and the size of AuNPs is lower. Ag NPs in the sample Ag/TiO<sub>2</sub> (cit) have the size distribution too wide for such comparison (see Figs. 6, 7 and Table 2). It seems to be caused by the secondary nucleation in these conditions [63].

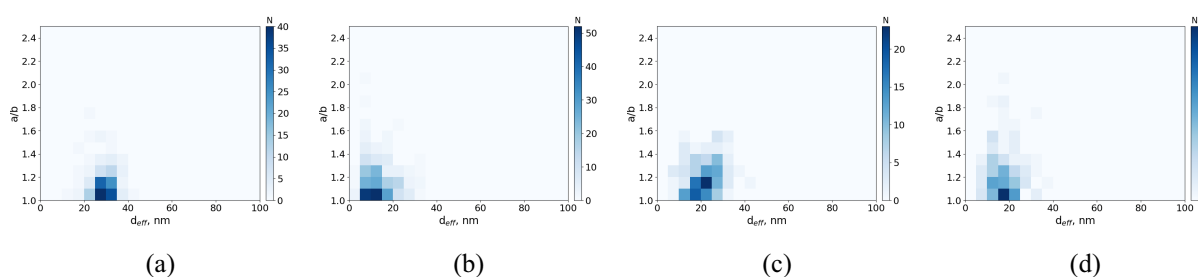


FIG. 6. 2D distributions of gold NPs in the Au/TiO<sub>2</sub> nanocomposites: (a) Au/TiO<sub>2</sub> (imp), (b) Au/TiO<sub>2</sub> (b), (c) Au/TiO<sub>2</sub> (cit), (d) Au/TiO<sub>2</sub> (UV)

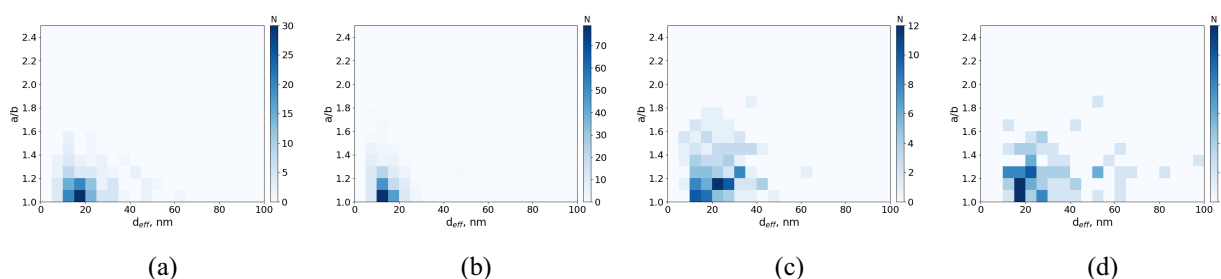


FIG. 7. 2D distributions of silver NPs in the Ag/TiO<sub>2</sub> nanocomposites: (a) Ag/TiO<sub>2</sub> (imp), (b) Ag/TiO<sub>2</sub> (b), (c) Ag/TiO<sub>2</sub> (cit), (d) Ag/TiO<sub>2</sub> (UV)

In the case of samples, obtained using UV irradiation, high anisotropy were expected due to a reduction of metal ions directly on the surface of titania, and, hence, the heterogeneous nucleation. According to the obtained data, NPs size and anisotropy distributions are similar to the particles, obtained by the citrate reduction. The number of particles of  $\geq 75$  nm in the Ag/TiO<sub>2</sub> (UV) and the corresponding value of  $k_{10\%}$  higher, that in the case of all the other samples, seems to be caused by the direct AgNO<sub>3</sub> decomposition in the solution under the UV irradiation. The metal NPs size and anisotropy distributions are presented on Figs. 7, and 6. Summarizing the TEM statistics results we conclude that the  $k$ -values, presented in the Table 2 may be used as an anisotropy descriptors, and according to the synthesis methods, allows one to estimate the quality of contact between titania and metal NPs.

#### 4.2. X-ray diffraction

The XRD demonstrates that all samples possess titania with initial anatase-rutile ratio, whereas gold and silver included in nanocomposites correspond only to *fcc* phases (Anatase (JCPDS Card no. 21-1272), Rutile (JCPDS Card no. 21-1276), Gold (JCPDS Card no. 4-784), Silver (JCPDS Card no. 4-783)). Using EDX analysis it

was confirmed that the metal content corresponds to the 5%w.p. Based on results of the XRD profile analysis, the coherent scattering regions (CSR) were calculated and shown in the Table 2. Being in the 10–25 nm range the calculated CSR sizes consistent with with the TEM data: samples, obtained by the borohydride reduction demonstrate the smaller CSR size of 7 nm in comparison with the case of reduction by citrate (14–17 nm). The CSR size for impregnated sample Au/TiO<sub>2</sub> (imp) is less that the same value for the Au/TiO<sub>2</sub> (cit) sample, obtained by the similar value in the presence of titania. Generally, the XRD results confirm the TEM data and hence we can consider the TEM statistics sufficient. For the NPs size relations for the samples Ag/TiO<sub>2</sub> (imp) and Ag/TiO<sub>2</sub> (cit) there are the difference between TEM data and the CSR sizes. These differences potentially caused by the significant anisotropy of the particles for the Ag/TiO<sub>2</sub> (cit) sample (see Fig. 7). Insufficient number of *fcc* metals peaks on the XRD patterns and overlapping of reflexes does not allow to resolve the anisotropy of CSR in this case (Fig. 8), therefore, the TEM data seems to be more informative here.

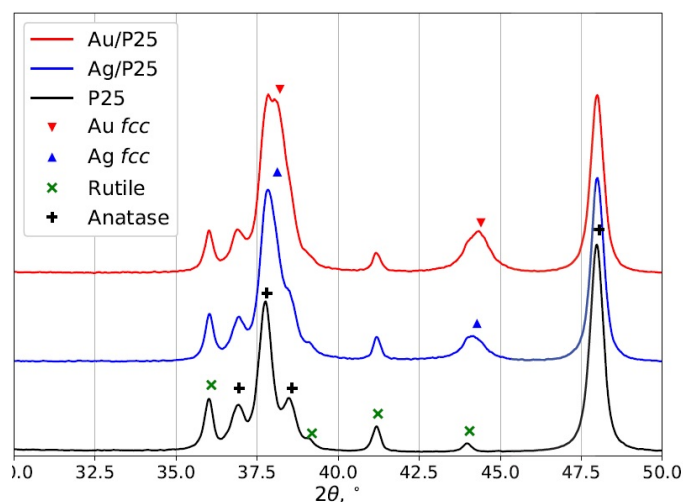


FIG. 8. XRD patterns of Au/TiO<sub>2</sub> (cit), Ag/TiO<sub>2</sub> (cit) nanocomposites and the initial Aeroxide P25

### 4.3. Optical properties

According to the eq. (1) the SPR peak position should be expected to shift to the higher wavelength range with the increase of the medium permittivity up to the value, corresponding to the core-shell metal@TiO<sub>2</sub> NPs. The results of DDA calculations are exemplified on the Fig. 9. Range of  $d_{eff}$  and anisotropy values were taken of 5–100 nm and 1–1.25 correspondingly to be representative for the previously calculated distributions (Figs. 6,7). It was shown that in the selected range of parameters, there are no significant changes of the SPR peak position, associated with the size and anisotropy effects. Meanwhile, broadening of the SPR peak increases with the anisotropy, which may indicates the contact formation analyzing optical absorption spectra. It should be noted, that the mean value of refractive index varies from one particle to another due to different quantity of neighboring titania particles. Therefore, the red shift of the SPR peak may be interpreted as a descriptor of the contact properties.

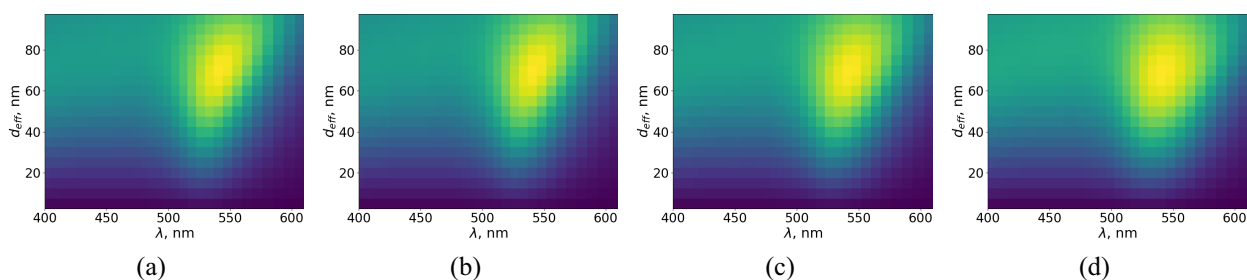


FIG. 9. Simulated absorption spectra for Au NPs with the  $d_{eff}$  value vary from 5 to 100 nm and the asymmetry coefficient of (a) 1, (b) 1.05, (c) 1.15 and (d) 1.25

UV-vis TRS allowed collection of optical absorption spectra, which are presented on the Fig. 10 and Fig. 11. According to this spectra, we can observe the presence of absorption edge at *ca.* 400 nm, which corresponds to the titania band gap. Since there are not shift of absorption edge position, initial titania matrix have not changed in the nanocomposites syntheses. In the range of 535–560 nm for the Au/TiO<sub>2</sub> nanocomposites and 435–455 nm for Au/TiO<sub>2</sub> nanocomposites we can find an intense SPR peak. The position of the SPR peaks are between the extinction maximums for metal NPs in air and in titania media, therefore, changing of the medium permittivity particularly effect on the spectra.

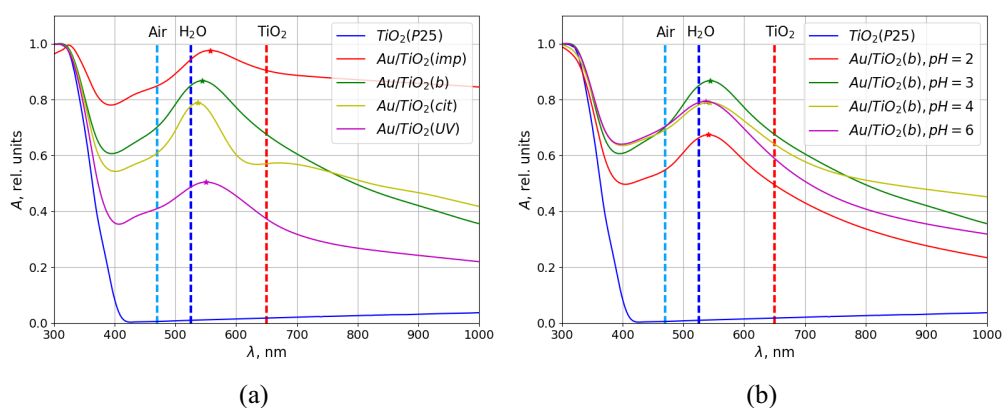


FIG. 10. Experimental absorption spectra for Au/TiO<sub>2</sub> nanocomposites: (a) synthesized by different reduction methods and (b) synthesized with borohydride reduction at different pH values. The vertical lines correspond to the simulated SPR peak positions at the different media

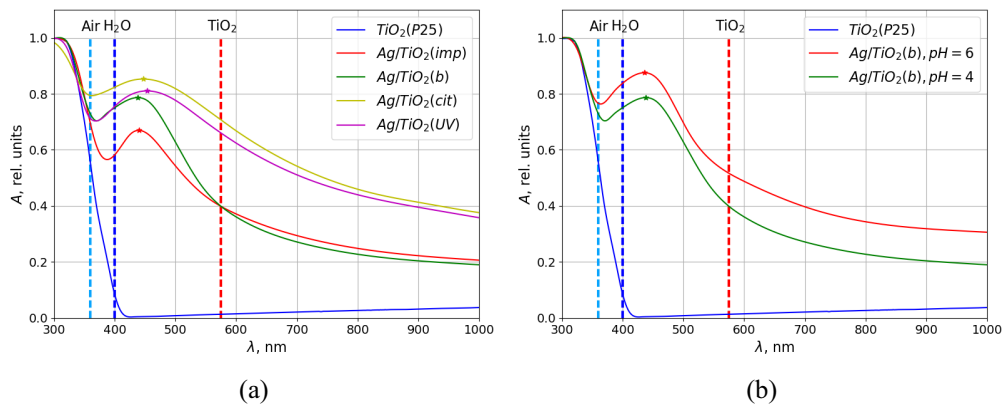


FIG. 11. Experimental absorption spectra for Ag/TiO<sub>2</sub> nanocomposites: (a) synthesized by different reduction methods and (b) synthesized with borohydride reduction at different pH values. The vertical lines correspond to the simulated SPR peak positions at the different media

According to the maximum of absorption presented in the Table 2 in the case of Ag/TiO<sub>2</sub> there is red shift of SPR peaks positions associated with slow reduction in UV and citrate assistance syntheses. As it was shown on the TEM data, the reduction rate affects on the anisotropy of metal NPs, and the quality of the contact with titania. According to the results of simulations for the measured range of sizes and anisotropy values, the red shift primarily caused by the formation of contact between titania and metal NPs. In the case of Au/TiO<sub>2</sub> nanocomposites, we also can observe similar behavior, however in the case of Au/TiO<sub>2</sub> (cit) nanocomposite the SPR peak position is lower than peak position of other nanocomposites. It may be caused by the side process of homogeneously nucleation in this case. The presence of a minor absorption peak at the 680–700 nm range may be interpreted as the evidence of the two different reduction processes.

For the silver NPs, the broad peaks are observed in the case of wide size distributions of NPs (Ag/TiO<sub>2</sub> (cit), Ag/TiO<sub>2</sub> (UV)), and for the gold NPs SPR peaks has a similar width, except the case of Au/TiO<sub>2</sub> (imp) sample, where the NPs aggregation additionally affects on the optical properties.

Comparing the absorption spectra of the nanocomposites obtained at different pH values using borohydride reduction (Fig. 10b and Fig. 11b), it should be noted that the SPR peak position shifts insignificantly. Therefore, in this case, the pH value does not affect on the absorption spectra or the nanocomposite morphology.

#### 4.4. Effect of synthesis method on the photocatalytic activity

The photocatalytic measurements were performed in phosphate buffer (pH 6.9) in the case of Au/TiO<sub>2</sub> nanocomposites, but in the case of Ag/TiO<sub>2</sub> nanocomposites the DW was used due the possibility of a silver phosphate formation during the photocatalytic process. The obtained PCA values are presented on the Table 3.

TABLE 3. The photocatalytic activity of nanocomposites

Sample	PCA *	Sample	PCA *
Au/TiO <sub>2</sub> (b)	190	Ag/TiO <sub>2</sub> (b)	200
Au/TiO <sub>2</sub> (cit)	270	Ag/TiO <sub>2</sub> (cit)	95
Au/TiO <sub>2</sub> (UV)	280	Ag/TiO <sub>2</sub> (UV)	100

\*PCA values correspond to the MO decoloration rate, normalized using eq. (8)

It should be noted that in the case of Au/TiO<sub>2</sub> nanocomposites series (Au/TiO<sub>2</sub> (b), Au/TiO<sub>2</sub> (cit), Au/TiO<sub>2</sub> (UV)) there is the improvement of PCA. These results very closely correlates with the initial assumption that slow reaction methods like UV and citrate reduction results in better contact formation. According to the TEM statistics data, the grade of contact is also associated with increasing of the anisotropy  $k$  values.

In front of this, in the case of Ag/TiO<sub>2</sub> nanocomposites similar behavior is not detected. Slow reduction methods and demonstrated above increasing of anisotropy do not lead to PCA improvement. Besides, the Ag/TiO<sub>2</sub>(b) nanocomposite demonstrate the twice increasing of PCA compared with initial titania, that may be caused by size effect. As it was reported in articles review (Table 1) small silver NPs, which we can observe in this case, possess shifted Fermi level, and hence metal/semiconductor contact turns to Schottky type. Therefore, the size effect dominates in the case of PCA of Ag/TiO<sub>2</sub> nanocomposites.

## 5. Conclusion

In this work, we demonstrated that the various synthetic methods allow one to obtain the Au/TiO<sub>2</sub> and Ag/TiO<sub>2</sub> nanocomposites with different morphology and properties. The use of different reducing agents results in the various quality of the contact between metal NPs and titania, that significant effects on the PCA. Nevertheless the direct observation of the contact properties is complicated, therefore the metal NPs anisotropy were suggested as a contact quality descriptor. We proposed the TEM-based quantitative method of anisotropy measurements with the use of statistical analysis. It was shown that the increase of anisotropy is likely caused by the interaction of metal NPs and titania in the synthetic process. Thus, in the case of the low reduction rate the better contact formation and the high anisotropy are observed.

The results of the PCA measurement demonstrated the opposite effects in the case of the Au/TiO<sub>2</sub> and Ag/TiO<sub>2</sub> nanocomposites, associated with different work functions of gold and silver. For the Au/TiO<sub>2</sub> nanocomposites, the positive effect of the contact on the PCA value was confirmed, and it correlates with the NPs anisotropy. In the case of Ag/TiO<sub>2</sub> nanocomposites the PCA increasing was detected only in the case of small NPs formation.

## Acknowledgements

The reported study was funded by RFBR according to the research project No 16-33-01044. This work was supported by M. V. Lomonosov Moscow State University Program of Development. Authors are grateful to Dr. O. A. Shlyakhtin for the fruitful discussions and assistance with the lyophilization.

## References

- [1] Chong M.N., Jin B., Chow C.W., Saint C. Recent developments in photocatalytic water treatment technology: A review. *Water Research*, 2010, **44**(10), P. 2997-3027.
- [2] Turchi C.S., Ollis D.F. Photocatalytic degradation of organic water contaminants: Mechanisms involving hydroxyl radical attack. *Journal of Catalysis*, 1990, **122**(1), P. 178-192.
- [3] Zaleska A., Hupka J., Wiergowski M., Biziuk M. Photocatalytic degradation of lindane, p,p-DDT and methoxychlor in an aqueous environment. *Journal of Photochemistry and Photobiology A: Chemistry*, 2000, **135**(23), P. 213-220.

- [4] Karthikeyan N., Narayanan V., Stephen A. Visible light degradation of textile effluent using nanostructured TiO<sub>2</sub>/Ag/CuO photocatalysts. *Nanosystems: Physics, Chemistry, Mathematics*, 2016, **7**(4), P. 695-698.
- [5] Abe R. Recent progress on photocatalytic and photoelectrochemical water splitting under visible light irradiation. *Journal of Photochemistry and Photobiology C: Photochemistry Reviews*, 2010, **11**(4), P. 179-209.
- [6] Habisreutinger S.N., Schmidt-Mende L., Stolarczyk J.K. Photocatalytic reduction of CO<sub>2</sub> on TiO<sub>2</sub> and other semiconductors. *Angewandte Chemie International Edition*, 2013, **52**(29), P. 7372-7408.
- [7] Carp O., Huisman C., Reller A. Photoinduced reactivity of titanium dioxide. *Progress in Solid State Chemistry*, 2004, **32**(12), P. 33-177.
- [8] Low J., Cheng B., Yu J. Surface modification and enhanced photocatalytic CO<sub>2</sub> reduction performance of TiO<sub>2</sub>: a review. *Applied Surface Science*, 2017, **392**, P. 658-686.
- [9] Kolesnik I.V., Chebotaeva G.S., Yashina L.V., Konstantinova E.A., Eliseev A.A., Lukashin A.V., Tretyakov Y.D. Preparation of Nanocrystalline Nitrogen-doped Mesoporous Titanium Dioxide. *Mendeleev Communications*, 2013, **23**(1), P. 11-13.
- [10] Maksimov V.D., Shapovov A.S., Ivanov V.K., Churagulov B.R., Tretyakov Y.D. Hydrothermal synthesis of nanocrystalline anatase from aqueous solutions of titanium sulfate for photocatalytic applications. *Theoretical Foundations of Chemical Engineering*, 2009, **43**(5), P. 713.
- [11] Meskin P.E., Gavrilov A.I., Maksimov V.D., Ivanov V.K., Churagulov B.P. Hydrothermal/microwave and hydrothermal/ultrasonic synthesis of nanocrystalline titania, zirconia, and hafnia. *Russian Journal of Inorganic Chemistry*, 2007, **52**(11), P. 1648-1656.
- [12] Trommer R.M., Bergmann C.P. et al. *Flame Spray Technology*. Springer-Verlag, Berlin, Heidelberg, 2015.
- [13] Moiseev A., Qi F., Deubener J., Weber A. Photocatalytic activity of nanostructured titanium dioxide from diffusion flame synthesis. *Chemical Engineering Journal*, 2011, **170**(1), P. 308-315.
- [14] Saekow S., Maiakgree W., Jarembon W., Pimanpang S., Amornkitbamrung V. High intensity UV radiation ozone treatment of nanocrystalline TiO<sub>2</sub> layers for high efficiency of dye-sensitized solar cells. *Journal of Non-Crystalline Solids*, 2012, **358**(17), P. 2496-2500. Proceedings of the 24-th International Conference on Amorphous and Nanocrystalline Semiconductors (ICANS 24) Nara, Japan August 21-26, 2011.
- [15] Lebedev V.A., Sudin V.V., Kozlov D.A., Garshev A.V. Photocatalytic properties of nanocrystalline TiO<sub>2</sub> modified with CuO and WO<sub>3</sub>. *Nanotechnologies in Russia*, 2016, **11**(1), P. 20-28.
- [16] Han T., Zhou D., Wang H., Zheng X. The study on preparation and photocatalytic activities of Cu<sub>2</sub>O/TiO<sub>2</sub> nanoparticles. *Journal of Environmental Chemical Engineering*, 2015, **3**(4), P. 24532462.
- [17] Tseng I.-H., Wu J. C.-S. Chemical states of metal-loaded titania in the photoreduction of CO<sub>2</sub>. *Catalysis today*, 2004, **97**(2), P. 113-119.
- [18] Koirala A.R., Docao S., Lee S.B., Yoon K.B. Fate of methanol under one-pot artificial photosynthesis condition with metal-loaded TiO<sub>2</sub> as photocatalysts. *Catalysis Today*, 2015, **243**, P. 235-250.
- [19] Logar M., Jančar B., Šturm S., Suvorov D. Weak polyelectrolyte multilayer-assisted in situ synthesis as a route toward a plasmonic Ag/TiO<sub>2</sub> photocatalyst. *Langmuir*, 2010, **26**(14), P. 12215-12224.
- [20] Evans J.E., Springer K.W., Zhang J.Z. Femtosecond studies of interparticle electron transfer in a coupled CdS-TiO<sub>2</sub> colloidal system. *The Journal of Chemical Physics*, 1994, **101**(7), P. 6222-6225.
- [21] Cushing S.K., Li J., Meng F., Senty T.R., Suri S., Zhi M., Li M., Bristow A.D., Wu N. Photocatalytic activity enhanced by plasmonic resonant energy transfer from metal to semiconductor. *Journal of the American Chemical Society*, 2012, **134**(36), P. 15033-15041.
- [22] Riviere J. The work function of gold. *Applied Physics Letters*, 1966, **8**(7), P. 172172.
- [23] Imanishi A., Tsuji E., Nakato Y. Dependence of the work function of TiO<sub>2</sub> (Rutile) on crystal faces, studied by a scanning auger microprobe. *The Journal of Physical Chemistry C*, 2007, **111**(5), P. 2128-2132.
- [24] Dweydari A., Mee C. Work function measurements on (100) and (110) surfaces of silver. *Physica Status Solidi (A)*, 1975, **27**(1), P. 223-230.
- [25] Schnippering M., Carrara M., Foelske A., Kötz R., Fermín D.J. Electronic properties of Ag nanoparticle arrays. A Kelvin probe and high resolution XPS study. *Physical Chemistry Chemical Physics*, 2007, **9**(6), P. 725-730.
- [26] Cozzoli P.D., Fanizza E., Comparelli R., Curri M.L., Agostiano A., Laub D. Role of metal nanoparticles in TiO<sub>2</sub>/Ag nanocomposite-based microheterogeneous photocatalysis. *The Journal of Physical Chemistry B*, 2004, **108**(28), P. 9623-9630.
- [27] Subramanian V., Wolf E.E., Kamat P.V. Catalysis with TiO<sub>2</sub>/gold nanocomposites. Effect of metal particle size on the Fermi level equilibration. *Journal of the American Chemical Society*, 2004, **126**(15), P. 4943-4950.
- [28] Liang Y.-C., Wang C.-C., Kei C.-C., Hsueh Y.-C., Cho W.-H., Perng T.-P. Photocatalysis of Ag-loaded TiO<sub>2</sub> nanotube arrays formed by atomic layer deposition. *The Journal of Physical Chemistry C*, 2011, **115**(19), P. 9498-9502.
- [29] Grabowska E., Zaleska A., Sorgues S., Kunst M., Etcheberry A., Colbeau-Justin C., Remita H. Modification of titanium (IV) dioxide with small silver nanoparticles: application in photocatalysis. *The Journal of Physical Chemistry C*, 2013, **117**(4), P. 1955-1962.
- [30] Zhang L., Yu J.C., Yip H.Y., Li Q., Kwong K.W., Xu A.-W., Wong P.K. Ambient light reduction strategy to synthesize silver nanoparticles and silver-coated TiO<sub>2</sub> with enhanced photocatalytic and bactericidal activities. *Langmuir*, 2003, **19**(24), P. 10372-10380.
- [31] Sung-Suh H.M., Choi J.R., Hah H.J., Koo S.M., Bae Y.C. Comparison of Ag deposition effects on the photocatalytic activity of nanoparticulate TiO<sub>2</sub> under visible and UV light irradiation. *Journal of Photochemistry and Photobiology A: Chemistry*, 2004, **163**(1), P. 37-44.
- [32] El-Kemary M., Abdel-Moneam Y., Madkour M., El-Mehasseb I. Enhanced photocatalytic degradation of Safranin-O by heterogeneous nanoparticles for environmental applications. *Journal of Luminescence*, 2011, **131**(4), P. 570-576.
- [33] Zhang H., Liang C., Liu J., Tian Z., Wang G., Cai W. Defect-mediated formation of Ag clusterdoped TiO<sub>2</sub> nanoparticles for efficient photodegradation of pentachlorophenol. *Langmuir*, 2012, **28**(8), P. 3938-3944.
- [34] Ko S., Banerjee C. K., Sankar J. Photochemical synthesis and photocatalytic activity in simulated solar light of nanosized Ag doped TiO<sub>2</sub> nanoparticle composite. *Composites Part B: Engineering*, 2011, **42**(3), P. 579-583.
- [35] Pan X., Xu Y.-J. Defect-mediated growth of noble-metal (Ag, Pt, and Pd) nanoparticles on TiO<sub>2</sub> with oxygen vacancies for photocatalytic redox reactions under visible light. *The Journal of Physical Chemistry C*, 2013, **117**(35), P. 17996-18005.
- [36] Xiang Q., Yu J., Cheng B., Ong H. Microwave-Hydrothermal Preparation and Visible-Light Photoactivity of Plasmonic Photocatalyst Ag-TiO<sub>2</sub> Nanocomposite Hollow Spheres. *ChemistryAn Asian Journal*, 2010, **5**(6), P. 1466-1474.
- [37] Wang Q., Yang X., Liu D., Zhao J. Fabrication, characterization and photocatalytic properties of Ag nanoparticles modified TiO<sub>2</sub> NTs. *Journal of Alloys and Compounds*, 2012, **527**, P. 106-111.

- [38] He X., Cai Y., Zhang H., Liang C. Photocatalytic degradation of organic pollutants with Ag decorated free-standing TiO<sub>2</sub> nanotube arrays and interface electrochemical response. *Journal of Materials Chemistry*, 2011, **21**(2), P. 475-480.
- [39] Zheng Z., Huang B., Qin X., Zhang X., Dai Y., Whangbo M.-H. Facile in situ synthesis of visible-light plasmonic photocatalysts M@TiO<sub>2</sub> (M= Au, Pt, Ag) and evaluation of their photocatalytic oxidation of benzene to phenol. *Journal of Materials Chemistry*, 2011, **21**(25), P. 9079-9087.
- [40] Shan Z., Wu J., Xu F., Huang F.-Q., Ding H. Highly effective silver/semiconductor photocatalytic composites prepared by a silver mirror reaction. *The Journal of Physical Chemistry C*, 2008, **112**(39), P. 15423-15428.
- [41] Liu C., Yang D., Jiao Y., Tian Y., Wang Y., Jiang Z. Biomimetic synthesis of TiO<sub>2</sub>/SiO<sub>2</sub>/Ag nanocomposites with enhanced visible-light photocatalytic activity. *ACS applied materials & interfaces*, 2013, **5**(9), P. 3824-3832.
- [42] Njoki P.N., Lim I.-I. S., Mott D., Park H.-Y., Khan B., Mishra S., Sujakumar R., Luo J., Zhong C.-J. Size correlation of optical and spectroscopic properties for gold nanoparticles. *The Journal of Physical Chemistry C*, 2007, **111**(40), P. 14664-14669.
- [43] Eustis S., El-Sayed M.A. Why gold nanoparticles are more precious than pretty gold: noble metal surface plasmon resonance and its enhancement of the radiative and nonradiative properties of nanocrystals of different shapes. *Chemical society reviews*, 2006, **35**(3), P. 209-217.
- [44] Zhao J., Pinchuk A. O., McMahon J.M., Li S., Ausman L.K., Atkinson A.L., Schatz G.C. Methods for describing the electromagnetic properties of silver and gold nanoparticles. *Accounts of chemical research*, 2008, **41**(12), P. 1710-1720.
- [45] Kelly K.L., Coronado E., Zhao L.L., Schatz G.C. The Optical Properties of Metal Nanoparticles: The Influence of Size, Shape, and Dielectric Environment. *The Journal of Physical Chemistry B*, 2003, **107**(3), P. 668-677.
- [46] Draine B.T., Flatau P.J. Discrete-dipole approximation for scattering calculations. *Journal of the Optical Society of America A*, 1994, **11**(4), P. 1491-1499.
- [47] Rakić A. D., Djurišić A. B., Elazar J. M., Majewski M.L. Optical properties of metallic films for vertical-cavity optoelectronic devices. *Applied optics*, 1998, **37**(22), P. 5271-5283.
- [48] Zhou M., Wang B., Rozynek Z., Xie Z., Fossum J.O., Yu X., Raaen S. Minute synthesis of extremely stable gold nanoparticles. *Nanotechnology*, 2009, **20**(50), P. 505606.
- [49] Chânet M., Micoud F., Roche I., Chânet E. Kinetics of sodium borohydride direct oxidation and oxygen reduction in sodium hydroxide electrolyte: Part I. BH<sub>4</sub><sup>-</sup> electro-oxidation on Au and Ag catalysts. *Electrochimica Acta*, 2006, **51**(25), P. 5459-5467.
- [50] Polyakov A.Y., Lebedev V.A., Shirshin E.A., Rumyantsev A.M., Volikov A.B., Zhrebker A., Garshev A.V., Goodilin E.A., Perminova I.V. Non-classical growth of water-redispersible spheroidal gold nanoparticles assisted by leonardite humate. *CrystEngComm*, 2017, **19**(5), P. 876-886.
- [51] Ojea-Jiménez I., Campanera J. M. Molecular Modeling of the Reduction Mechanism in the Citrate-Mediated Synthesis of Gold Nanoparticles. *The Journal of Physical Chemistry C*, 2012, **116**(44), P. 23682-23691.
- [52] Kumar S., Gandhi K.S., Kumar R. Modeling of Formation of Gold Nanoparticles by Citrate Method. *Industrial & Engineering Chemistry Research*, 2007, **46**(10), P. 3128-3136.
- [53] Petříček V., Dušek M., Palatinus L. Crystallographic Computing System JANA2006: General features. *Zeitschrift für Kristallographie - Crystalline Materials*, 2014, **229**(5), P. 345-352.
- [54] Nečas D., Klapetek P. Gwyddion: an open-source software for SPM data analysis. *Central European Journal of Physics*, 2012, **10**(1), P. 181-188.
- [55] Jones E., Oliphant T., Peterson P. et al. SciPy: Open source scientific tools for Python. 2001. URL: <http://www.scipy.org/>.
- [56] Hunter J. D. Matplotlib: A 2D graphics environment. *Computing In Science & Engineering*, 2007, **9**(3), P. 90-95.
- [57] Lebedev V., Kozlov D., Kolesnik I., Poluboyarinov A., Becerikli A., Grünert W., Garshev A. The amorphous phase in titania and its influence on photocatalytic properties. *Applied Catalysis B: Environmental*, 2016, **195**, P. 39-47.
- [58] Chen H.Y., Zahraa O., Bouchy M. Inhibition of the adsorption and photocatalytic degradation of an organic contaminant in an aqueous suspension of TiO<sub>2</sub> by inorganic ions. *Journal of Photochemistry and Photobiology A Chemistry*, 1997, **108**(1), P. 37-44.
- [59] Chen F., Zhao J., Hidaka H. Adsorption factor and photocatalytic degradation of dye-constituent aromatics on the surface of TiO<sub>2</sub> in the presence of phosphate anions. *Research on chemical intermediates*, 2003, **29**(7-9), P. 733-748.
- [60] Zhao D., Chen C., Wang Y., Ji H., Ma W., Zang L., Zhao J. Surface Modification of TiO<sub>2</sub> by Phosphate: Effect on Photocatalytic Activity and Mechanism Implication. *The Journal of Physical Chemistry C*, 2008, **112**(15), P. 5993-6001.
- [61] Polyakov A.Y., Lebedev V., Yadgarov L., Goodilin E. Two facile routes for functionalization of WS<sub>2</sub> nanotubes with silver nanoparticles. *Nanosystems: Physics, Chemistry, Mathematics*, 2017, **8**(5), P. 628-634.
- [62] Tian Y., Tsuma T. Mechanisms and applications of plasmon-induced charge separation at TiO<sub>2</sub> films loaded with gold nanoparticles. *Journal of the American Chemical Society*, 2005, **127**(20), P. 7632-7637.
- [63] Gorup L.F., Longo E., Leite E.R., Camargo E.R. Moderating effect of ammonia on particle growth and stability of quasi-monodisperse silver nanoparticles synthesized by the Turkevich method. *Journal of Colloid and Interface Science*, 2011, **360**(2), P. 355-358.